TOPICAL REVIEW — High pressure physics

Unreacted equation of states of typical energetic materials under static compression: A review*

Zhaoyang Zheng(郑朝阳)[1,2] and Jijun Zhao(赵纪军)[1,†]

[1] *Key Laboratory of Materials Modification by Laser, Ion and Electron Beams (Dalian University of Technology), Ministry of Education, Dalian* 116024, *China*

[2] *National Key Laboratory of Shock Wave and Detonation Physics, Institute of Fluid Physics, China Academy of Engineering Physics, Mianyang* 621900, *China*

(Received 23 June 2015; revised manuscript received 22 July 2015; published online 27 May 2016)

The unreacted equation of state (EOS) of energetic materials is an important thermodynamic relationship to characterize their high pressure behaviors and has practical importance. The previous experimental and theoretical works on the equation of state of several energetic materials including nitromethane, 1,3,5-trinitrohexahydro-1,3,5-triazine (RDX), 1,3,5,7-tetranitro-1,3,5,7-tetrazacyclooctane (HMX), hexanitrostilbene (HNS), hexanitrohexaazaisowurtzitane (HNIW or CL-20), pentaerythritol tetranitrate (PETN), 2,6-diamino-3,5-dinitropyrazine-1-oxide (LLM-105), triamino-trinitrobenzene (TATB), 1,1-diamino-2,2-dinitroethene (DADNE or FOX-7), and trinitrotoluene (TNT) are reviewed in this paper. The EOS determined from hydrostatic and non-hydrostatic compressions are discussed and compared. The theoretical results based on *ab initio* calculations are summarized and compared with the experimental data.

Keywords: energetic material, equation of state, bulk modulus, compression

PACS: 62.50.–p, 31.15.A–, 66.70.Lm, 64.30.–t **DOI:** 10.1088/1674-1056/25/7/076202

1. Introduction

Energetic materials are a class of materials that can release heat and (or) gaseous products at a high rate upon stimulus by heat, shock, impact, spark, etc. They can be classified as explosives, propellants, and pyrotechnics and are widely used for military and constructional purposes.[1] Their accurate thermodynamic parameters under extreme conditions are very helpful for their safe storage, transport, and usage. Under high pressure and (or) high temperature, many physical and chemical properties of energetic materials should be characterized, such as polymorphic behavior, decomposition, detonation, etc. There have been a few comprehensive reviews of experimental and theoretical studies on these properties.[1–4]

An important problem for energetic materials is to understand their behavior under high pressure. In this paper, the response of energetic materials to high compression is discussed according to the pressure–volume (P–V) data from experimental measurement and (or) *ab initio* calculation. The P–V relationship can be described as equation of state (EOS) in thermodynamics. Then a key parameter called bulk modulus can be evaluated by combining the P–V data with the EOS. Here, the isotherms and bulk moduli of several typical energetic materials (see Fig. 1) including nitromethane, 1,3,5-trinitrohexahydro-1,3,5-triazine (RDX), 1,3,5,7-tetranitro-1,3,5,7-tetrazacyclooctane (HMX), hexanitrostilbene (HNS), hexanitrohexaazaisowurtzitane (HNIW or CL-20), pentaerythritol tetranitrate (PETN), 2,6-diamino-3,5-dinitropyrazine-1-oxide (LLM-105), triamino-trinitrobenzene (TATB), 1,1-diamino-2,2-dinitroethene (DADNE or FOX-7), and trinitrotoluene (TNT) are summarized.

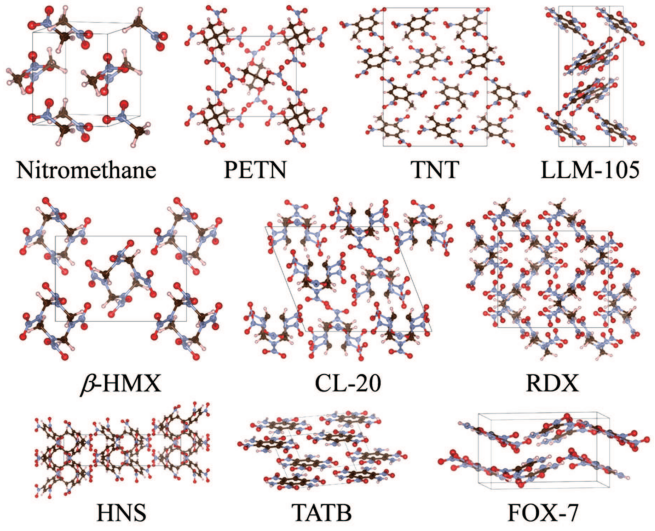


Fig. 1. Crystal structures of typical energetic materials.

2. Equation of state

Equation of state is a relationship between state variables in physics and thermodynamics. It can be a constitutive equa-

*Project supported by the National Natural Science Foundation of China (Grant Nos. 11174045 and 11404050).

†Corresponding author. E-mail: zhaojj@dlut.edu.cn

© 2016 Chinese Physical Society and IOP Publishing Ltd

tion, describing the relationship between several state functions of the materials, such as pressure P, volume V, temperature T, and internal energy E. Here we give several typical formulas of EOS as follows.

Firstly, the bulk modulus at constant temperature is defined by

$$B = -V\left(\frac{\partial P}{\partial V}\right)_T. \tag{1}$$

By assuming the bulk modulus is a linear function of pressure, then the Murnaghan equation can be derived and written as[5]

$$P(V) = \frac{B_0}{B'}\left[\left(\frac{V}{V_0}\right)^{-B'} - 1\right], \tag{2}$$

where B_0 is the bulk modulus at zero pressure, B' is the pressure derivative of B_0, and V_0 is the equilibrium volume. Note that one assumes that B' is a constant in the Murnaghan equation and is set to 4.0 in most cases. Thus it is unlikely to describe the high pressure behavior for the cases where B' changes with pressure.

In order to remedy the disadvantage, Birch modified the Murnaghan equation using the finite strain theory and derived the Birch–Murnaghan equation.[6] A finite strain is defined as

$$f = \frac{1}{2}\left[\left(\frac{V}{V_0}\right)^{-2/3} - 1\right]. \tag{3}$$

Then the Helmholtz free energy F can be written as

$$F = af^2 + bf^3 + cf^4 + \cdots. \tag{4}$$

According to the relation between P and F, the 2nd and the 3rd Birch–Murnaghan EOS are given as

$$P(V) = \frac{3B_0}{2}\left[\left(\frac{V_0}{V}\right)^{7/3} - \left(\frac{V_0}{V}\right)^{5/3}\right], \tag{5}$$

$$P(V) = \frac{3B_0}{2}\left[\left(\frac{V_0}{V}\right)^{7/3} - \left(\frac{V_0}{V}\right)^{5/3}\right] \times \left\{1 + \frac{3}{4}(B' - 4)\left[\left(\frac{V_0}{V}\right)^{2/3} - 1\right]\right\}. \tag{6}$$

Apart from these two mostly used EOS, there are many other equations, such as the Vinet equation[7] and the Poirier–Tarantola (PT) logarithmic equation,[8] which are respectively defined as

$$P(V) = 3B_0\left(\frac{V_0}{V}\right)^{2/3}\left[1 - \left(\frac{V_0}{V}\right)^{-1/3}\right] \times \exp\left\{-\frac{3}{2}(B' - 1)\left[\left(\frac{V_0}{V}\right)^{-1/3} - 1\right]\right\}, \tag{7}$$

$$P(V) = B_0\frac{V_0}{V}\left\{\ln\left(\frac{V_0}{V}\right) + \frac{B' - 2}{2}\left[\ln\left(\frac{V_0}{V}\right)^2\right]\right\}. \tag{8}$$

Note that the Vinet EOS is considered to be a more realistic model under large compression.[9,10]

3. EOS of several energetic materials

3.1. Nitromethane

Nitromethane is an important prototype explosive. To date, there have been many studies on the isotherms of nitromethane in both solid and liquid states. Experimentally, Lysne and Hardesty performed shock compression to obtain the Hugoniots and isotherms of liquid nitromethane up to 10 GPa.[11] For solid nitromethane, Cromer and his colleagues first reported its isotherm in the hydrostatic compression of 0.3–6.0 GPa using single crystal x-ray diffraction (XRD).[12] By fitting the P–V curve to the Murnaghan EOS, B_0 and B' were determined to be 7.0 GPa and 5.7, respectively. Later, Yanger and Olinger re-determined the isotherm up to 15 GPa at room temperature using the similar technique.[13] They used a model including the shock and particle velocities to fit the P–V data and obtained $B_0 = 10.1$ GPa at ambient conditions. Table 1 summarizes the EOS parameters of solid nitromethane from both experiments and *ab initio* calculations.

Recently, Citroni *et al.*[14] obtained the isotherm of solid nitromethane using angle dispersion x-ray diffraction below 27.3 GPa, which approaches its reaction threshold pressure. The results show that the B_0 and B' using the Murnaghan EOS are 8.3±0.2 GPa and 5.9±0.1, respectively, which are in perfect agreement with the previous experimental values.[12] But when the Vinet EOS is used to evaluate these values, the B_0 and B' are 8.3±0.3 GPa and 7.4±0.3, respectively, for the pressure above 15 GPa.

Theoretically, the structural properties of solid nitromethane under hydrostatic pressure up to 20 GPa have been investigated using density functional theory (DFT) with PBE functional by Liu *et al.*[15] The calculated isotherm agrees well with the experimental data.[12] The Murnaghan EOS gives $B_0 = 5.37$ GPa from the P–V data of 0–6 GPa and 6.37 GPa from that of 0–15 GPa, which are a little smaller than the experimental values.[12,13] They attributed the error to poor description of vdW interaction by DFT-PBE calculations. Zerilli, Hooper, and Kuklja studied the mechanical compressibility of solid nitromethane using both Hartree–Fock (HF) and DFT.[16] The results show that the HF calculations with a 6-21G basis set and uncorrected for basis set superposition error (BSSE) give the best agreement with the experimental data[13] due to the cancellation of BSSE with dispersion force errors. Moreover, Mota and Cagin analyzed the energy–volume (E–V) behavior of solid nitromethane using DFT within PBE functional.[17] By fitting these data to the 4th BM EOS, the calculated B_0 is 9.95 GPa, in agreement with the experimental value of 10.1 GPa.[13]

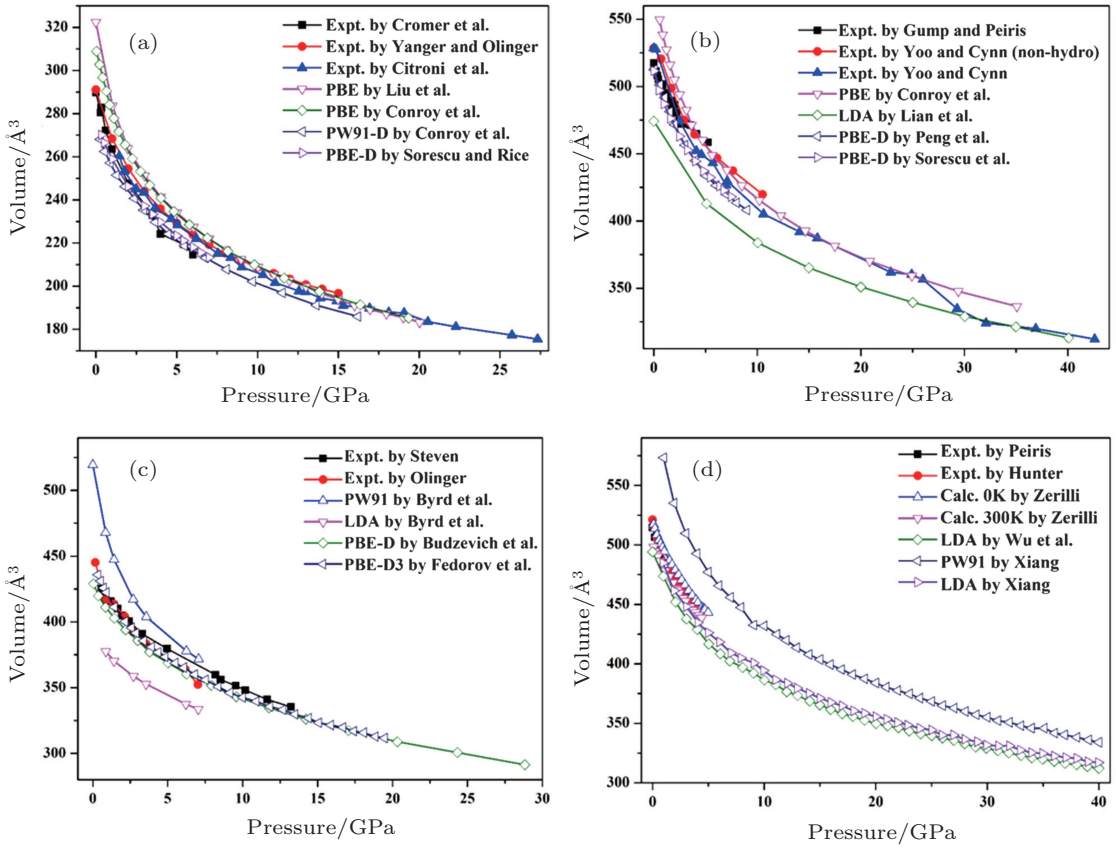


Fig. 2. Examples of experimental and theoretical isotherms of (a) nitromethane, (b) β-HMX, (c) TATB, and (d) FOX-7.

Table 1. Isothermal EOS parameters for nitromethane using different methods. RT stands for room temperature.

Method	T/K	P/GPa	EOS	B_0/GPa	B'
Expt.[12]	RT	0.3–6.0	Murnaghan	7.0	5.7
Expt.[13]	RT	0–15	–	10.1	–
Expt.[14]	RT	0–27.3	Murnaghan	8.3±0.2	5.9±0.1
		15–27.3	Vinet	8.3±0.3	7.4±0.1
DFT-PBE.[15]	0	0–6	Murnaghan	5.37	–
		0–15	Murnaghan	6.37	–
Calc.[17]	0	0–3.0	4$^{\text{th}}$ BM	9.95	–
DFT-PBE.[18]	0	$V/V_0 = 0.7$–1.0	Murnaghan	8.0	–
PW91-D.[18]			Murnaghan	12.9	–
B3LYP-D.[21]	0	–	–	14.6	8.1

Interestingly, Conroy *et al.* reported the EOS of solid nitromethane under both hydrostatic and uniaxial compression using DFT with and without empirical van der Waals (vdW) correction.[18] The results show that the error of the lattice constants for standard DFT is 2%–6%, but reduces to less than 1% after vdW correction. For the P–V curve, DFT with vdW correction agrees well with more recent experimental data[14] under low pressure, while the standard DFT agrees well under high pressure (see Fig. 2(a)). It has been confirmed by subsequential calculation by Sorescu and Rice.[19] Using the Murnaghan EOS, the calculated B_0 is 8.0 GPa for standard DFT and 12.9 GPa for DFT with vdW correction. They are in reasonable agreement with the experimental values ranging from 7.0 GPa to 10.1 GPa.[12–14] Under uniaxial compression, they observed the anisotropic behavior in shear stresses and predicted that the $\langle 001 \rangle$ direction has the greater sensitivity due to greater shear stress, which is consistent with Dick's model.[20] Recently, Slough and Perger calculated the bulk modulus of solid nitromethane from the elastic constants by DFT-D method.[21] The calculated value is 14.6 GPa using the 6-311G(d,p) basis set, moderately higher than the experimental values of 7.0–10.1 GPa.[12–14]

3.2. HMX

1,3,5,7-tetranitro-1,3,5,7-tetrazacyclooctane (HMX) is one of the most widely used explosives. Under the ambient conditions, there are three polymorphs (α, β, and δ), and the most stable phase is the β-HMX. Table 2 summarizes the EOS parameters of HMX from both experiments and *ab initio* calculations. In 1999, Yoo and Cynn[22] first studied the high-pressure behavior by determining the P–V relation of β-HMX using angle-resolved synchrotron XRD under quasi-hydrostatic conditions up to 45 GPa and non-hydrostatic conditions up to 10 GPa. Their results revealed that the high-pressure behavior of β-HMX strongly depends on the stress conditions. Under hydrostatic conditions, they obtained $B_0 = 12.4$ GPa and $B' = 10.4$ by fitting the P–V data using the 3$^{\text{rd}}$ BM equation in the pressure range of 0–27 GPa.

Note that they suggested that there may be a phase transition with an abrupt volume change of 4% at 27 GPa. But under non-hydrostatic conditions, the chemical reactions occur above 10 GPa. Thus, B_0 and B' in the pressure range of 0–10 GPa are 14.4 GPa and 13.3, respectively. This means that β-HMX is more compressible under hydrostatic conditions than that under non-hydrostatic conditions. They attributed it to chemical reactions occurring under non-hydrostatic conditions. Besides, the static isotherm is in good agreement with the shock Hugoniot, suggesting little temperature effect on the P–V relation.

Later, Gump and Peiris reported the temperature effect on the P–V data of β-HMX under both hydrostatic and non-hydrostatic compressions.[23] The B_0 and B' were calculated by fitting the P–V relation using the 3rd BM EOS. Under hydrostatics compression, the B_0 decreases from 21.0±1.02 GPa to 13.5±0.56 GPa as the temperature increases from 303 K to 413 K, which means that the compressibility of β-HMX increases with increasing temperature. However, the B_0 was calculated to be 14.8±0.56 GPa under non-hydrostatic compression at 303 K. Note that the B_0 decreases from 21.0±1.02 GPa for the hydrostatic case to 14.8±0.56 GPa for the non-hydrostatic situation. This trend is consistent with the previous result by Yoo and Cynn.[22]

Table 2. Isothermal EOS parameters for HMX using different methods. NH stands for non-hydrostatic.

Form	Method	T/K	P/GPa	EOS	B_0/GPa	B'
β-HMX	Expt.[22]	273	0–45	3rd BM	12.4	10.4
		273	0–10 (NH)	3rd BM	14.4	13.3
		303	0–5.8 (NH)	3rd BM	14.8±0.56	20.7±1.73
β-HMX	Expt.[23]	303	0–5.8	3rd BM	21.0±1.02	7.45±0.95
		373	0–5.8	3rd BM	14.1±0.82	11.6±1.41
		413	0–5.8	3rd BM	13.5±0.56	9.0±0.85
β-HMX	PBE.[26,27]	0	$V/V_0 = 0.7$–1.0	3rd BM	9.8	9.1
β-HMX	HF.[28]	0	$(V/V_0)^{1/3} = 0.92$–1.02	–	18.4	–
	HF.[29]	300		–	14.2	
BCHMX	MD.[30]	5	–	–	10.95	–
		273	–	–	6.1	–
β-HMX	LDA.[33]	0	0–40	Murnaghan	6.18	10.44
β-HMX	GGA.[33]	0	0–40	Murnaghan	21.1	10.34
β-HMX	LDA.[31]	0	0–30	Murnaghan	13.07	–
β-HMX	PBE.[36]	0	0–40	4th PT	12.5	9.9
β-HMX	vdW-DF.[39]	0	–	Murnaghan	15.82	8.06
α-HMX	vdW-DF.[39]	0	–	Murnaghan	14.91	7.39

Compared with the small amount of experimental works, there have been many more theoretical simulations to study the high-pressure behavior of HMX crystal. Byrd and Rice obtained the structural properties of β-HMX under hydrostatic pressure of 0–7.47 GPa using DFT within PW91, PBE, and LDA functionals.[24] They pointed out that LDA underestimates the cell volume, while both PW91 and PBE overestimate it in the calculated pressure range compared to the experiment values.[25] However, the difference between LDA and GGA diminishes as the pressure increases. In particular, the volumes obtained by PW91 and PBE approach the experimental values at pressure higher than 6–7 GPa, and converge to the same value as the pressure increases. The error of the cell volume, especially at low pressure, comes from the mistreatment of the vdW interaction, and one should be cautious when LDA and GGA are employed to interpret the calculated results.

Conroy and his colleagues studied the constitutive relationships of β-HMX under compression up to $V/V_0 = 0.7$ using DFT with PBE functional.[26,27] Their results show that the isothermal EOS is in reasonable agreement with the experimental values.[22] By using the 3rd BM EOS, the B_0 is 9.8 GPa, consistent with the experimental values of 12.4–21.0 GPa.[22,23] Under non-hydrostatic compression, a correlation between shear stresses and sensitivity was built by comparing the uniaxial compression data with the experimental information on the anisotropy in sensitivity to shock-induced detonation for PETN-I. The more sensitive the direction is, the greater the shear stresses are. Thus, they predicted that the anisotropy effect[27] may lead to anisotropy of the elastic–plastic shock transition and $\langle 110 \rangle$ and $\langle 010 \rangle$ directions may be more sensitive to initiation for β-HMX.[26]

Zerilli and Kuklja simulated the compression curve for β-HMX under the compression of $(V/V_0)^{1/3} = 0.92$–1.02 using HF approximation.[28] The results show that the isotherm also coincides well with the experimental curve.[22,23] They evaluated the bulk modulus using the usual thermodynamics relation and obtained $B_0 = 18.4$ GPa, in agreement with the experimental values of 12.4–21.0 GPa.[22,23] Later, they studied the effect of temperature on the EOS of β-HMX under hydrostatic pressures of 0–10 GPa and at the temperatures of 0–

400 K using first-principles calculations coupled with thermal vibrational energy to free energy.[29] The calculated isothermal EOS at 300 K agrees well with the experimental P–V data[22,23] (see Fig. 2(b)). They also found that the isothermal bulk modulus is relatively insensitive to the temperature change at constant volume, but sensitive to the temperature at constant pressure. The calculated B_0 is 14.2 GPa at 300 K and ambient pressure, in agreement with the experimental values ranging from 12.4 GPa to 21 GPa at ambient conditions.[22,23]

Xiao's group performed DFT calculations to study the isotherm for solid bicyco-HMX (BCHMX) under hydrostatic pressure of 0–400 Ga.[30] Their DFT results show that the compressibility is anisotropic: the structure along the a and b directions is much stiffer than that along the c direction due to larger compression in the c axis than that in the a and b axes. Besides, they also performed classical molecular dynamics to study the effects of temperature on isotherm for BCHMX in the temperature range of 5–400 K.[30] The bulk modulus can be obtained from the Lame coefficient (λ and μ) according to $B_0 = \lambda + 2\mu/3$, where $\lambda = C_{12}$ and $\mu = (C_{11} - C_{12})/2$. The results show that the B_0 decreases from 10.95 GPa to 3.8 GPa as the temperature increases from 5 K to 400 K, which means that the compressibility of BCHMX increases as the temperature increases. Later, they investigated the pressure effect on the structural properties of β-HMX under hydrostatic pressure of 0–100 GPa using DFT calculations.[31] LDA (PW91) underestimated (overestimated) the lattice constants compared with experiments,[22,23] consistent with their previous works.[32] But the difference between the lattice constants by LDA and those by PW91 gradually decreases as the pressures increase. Thus they pointed out that DFT can well describe the intermolecular interactions in HMX under high pressure. Moreover, they also found that the compressibility of HMX is anisotropic, in agreement with experimental reports[22,23] and theoretical finding.[30] By fitting the P–V data to the Murnaghan EOS below 30 GPa, the B_0 from the LDA calculation is 13.07 GPa, close to the experimental value of 12.4 GPa.[22]

Lu and his colleagues simulated the structural properties of β-HMX up to 40 GPa with DFT within LDA and GGA.[33] The P–V relation was obtained and showed that the volume compression $V/V_0 = 56.1\%$ for GGA and 66.2% for LDA up to 40 GPa. Both of the P–V curves reproduce roughly the trend of experimental observation. The calculated bulk moduli by LDA and GGA are 6.18 GPa and 21.1 GPa, respectively, by fitting the Murnaghan EOS. Later, Lian *et al*. studied the high pressure behavior of β-HMX up to 40 GPa with DFT within LDA.[34] They pointed out that LDA underestimates the cell volume by 8.78%, in agreement with the previous theoretical work.[32] In addition, the calculated EOS reveals the same trend as the results from Monte Carlo simulation.[35] Moreover, Cui and his colleagues obtained the bulk modulus of solid β-HMX under high pressure of 0–40 GPa using first-principles calculation.[36,37] The trend of the P–V curve was roughly consistent with that observed in experiments[22,23] and other simulations.[35] The calculated B_0 is 12.5 GPa by fitting the 4$^{\text{th}}$ PT EOS,[8] in good agreement with the experiment data of 12.4–21.0 GPa at ambient conditions.[22,23]

Chen *et al.* simulated the EOS of δ-HMX by DFT calculation and compared with that of β-HMX.[38] They showed the E–V and P–V curves. The results show that the calculated elastic constants and P–V data of β-HMX are compared with the experimental values.[22,23] According to the BM EOS, the B_0 for β-HMX is 11.7 GPa, in agreement with the experimental value (12.4 GPa).[22] The B_0 of 14.7 GPa was predicted for δ-HMX. Furthermore, Long and Chen built a physical model to describe the phonon density of state for HMX to calculate the thermodynamic properties including bulk modulus and Hugoniot curve.[39] The results are in good agreement with available experiments[22,23,40] at low pressure. The Murnaghan EOS gives $B_0 = 14.9$ GPa for α-HMX and 15.8 GPa for β-HMX.

Recently, Peng *et al.* studied the EOS of β-HMX under hydrostatic pressures up to 100 GPa using DFT-D2 method which includes an empirical vdW correction.[41] The results show that DFT-D2 could reproduce the hydrostatic-compression experimental data,[22,23] in agreement with the previous calculation by Sorescu and Rice.[19] Hence the vdW interaction is critically important in modeling the mechanical properties of β-HMX.

3.3. RDX

1,3,5-trinitrohexahydro-1,3,5-triazine (RDX) is also one of the commonly used explosives. The isotherms of α-RDX and γ-RDX have been explored using XRD and neutron diffraction up to 8 GPa by Oswald *et al.*[42] The bulk moduli are 10.0 GPa for α-RDX and 8.73 GPa for γ-RDX.

Theoretically, Zhao *et al.* reported the isotherm of RDX crystal under hydrostatic pressure of 0–3.65 GPa using DFT within GGA.[43] The calculated trend of the P–V relation is in agreement with the experiments.[25] Using the Murnaghan EOS, they obtained $B_0 = 8.04$ GPa, which is only 2/3 of the experimental value of 12.61 GPa,[25] indicating that GGA underestimates the stiffness of the RDX crystal. Later, Byrd and Rice calculated the structural properties of RDX under hydrostatic pressure of 0–3.95 GPa using DFT within

PW91, PBE, and LDA functional.[24] The results are similar to that for β-HMX. Moreover, Conroy *et al.* studied the anisotropic constitutive relationships of α-RDX using first-principles calculation.[44] They found that the error for the equilibrium properties is within 2%–3% compared with the experimental values. The calculated B_0 for α-RDX is 10.1 GPa, consistent with the experimental data of 12.61 GPa.[25] Besides, the data from uniaxial compression indicate that the anisotropy of structural and electronic properties may play a role for α-RDX under shock loading.

Table 3. Isothermal EOS parameters for RDX using different methods.

Form	Method	T/K	P/GPa	EOS	B_0/GPa	B'
α-RDX	Expt.[42]	273	0–4.0	3rd BM	10.0	11.3
γ-RDX	Expt.[42]	273	0–8.0	3rd BM	8.73	11.26
α-RDX	PW91.[43]	0	0–3.65	Murnaghan	8.04	7.97
α-RDX	PBE.[44]	0	$V/V_0 = 0.7$–1.0	3rd BM	10.1	8.4
				Vinet	10.3	7.9
α-RDX	DFT-D.[45]	0	0–5	3rd BM	15.54	6.46
γ-RDX	DFT-D.[45]	0	0–5	3rd BM	9.17	12.63
ε-RDX	DFT-D.[45]	0	0–5	3rd BM	10.63	12.32

Recently, DFT-D method has been used to calculate the EOS of RDX crystals by Hunter *et al.*[45] The calculated EOS of α-RDX, β-RDX, and ε-RDX are in excellent agreement with the experiment data.[42,46] It agrees with the previous calculation on RDX by Sorescu and Rice.[19] The 3rd BM EOS from the data of DFT-D calculations gives $B_0 = 15.54$ GPa for α-RDX, 9.67 GPa for β-RDX, and 10.63 GPa for γ-RDX, which are in good agreement with the previous experimental values of 10.10 GPa for α-RDX,[42] 9.50 GPa for β-RDX,[42] and 10.34 GPa for γ-RDX.[46] Thus, the DFT-D model is able to describe accurately the vdW interaction of RDX. The EOS parameters of RDX are summarized in Table 3 for both experiments and *ab initio* calculations.

3.4. LLM-105

2,6-diamino-3,5-dinitropyrazine-1-oxide (LLM-105) is a new kind of energetic material, which has performance and insensitivity between those of HMX and TATB. In experiments, Gump and his colleagues investigated the isothermal EOS of LLM-105 in the pressure range of 0–5.4 GPa at room temperature and 100 °C using synchrotron angle-dispersive XRD experiments.[47] No phase transition of LLM-105 was observed under hydrostatic compression up to 5.4 GPa at room temperature. They pointed out that the diffraction peaks return to those of the original ambient pressure after the pressure is released, suggesting that it is a reversible compression process. Meanwhile, the b axis is more compressible than the a and c axes. By fitting the 3rd BM EOS at ambient temperature, the B_0 and B' are 11.19±0.02 GPa and 18.54±0.04, respectively. The EOS parameters of LLM-105 are summarized in Table 4 for both experiments and *ab initio* calculations. Besides, the behavior of LLM-105 at 100 °C is similar to that at ambient temperature. The 4th BM EOS fit to the P–V data at 100 °C yields $B_0 = 6.37 \pm 0.05$ GPa and $B' = 9.3 \pm 0.3$, which are smaller than those at ambient temperature. This implies that the compressibility of LLM-105 increases with temperature, whose trend is identical to that of ε-CL-20.[48] Later, they obtained the isothermal EOS of LLM-105 at 180 °C in the pressure range of 0–5.4 GPa using the same method,[49] compared to that at ambient temperature and 100 °C. The isotherm and bulk modulus at ambient temperature and 100 °C are the same as their previous experimental results.[47] Then they used the Vinet EOS to fit the P–V data and obtained $B_0 = 12.52 \pm 0.01$ GPa and $B' = 12.9 \pm 0.02$ at ambient temperature, $B_0 = 5.33 \pm 0.005$ GPa and $B' = 18.78 \pm 0.02$ at 100 °C. Furthermore, they pointed out that no evidence is observed for phase transition up to 5 GPa at 180 °C and the b axis is still the most compressible direction among the three axes. The B_0 and B' were calculated to be 0.74±0.01 GPa and $B' = 233 \pm 29$ from the 3rd BM EOS, but $B_0 = 2.97 \pm 0.003$ GPa and $B' = 25.36 \pm 0.02$ from the Vinet EOS. The value of B' from the BM EOS significantly deviates from that from the Vinet EOS fit and the larger error is in line with the previous report,[9] which shows that the Vinet EOS is more accurate at higher compression and for highly compressible materials. Therefore, LLM-105 becomes more compressible with the temperature increasing.

Table 4. Isothermal EOS parameters for LLM-105 using different methods.

Method	T/K	P/GPa	EOS	B_0/GPa	B'
Expt.[47]	273	0-5.4	3rd BM	11.19±0.02	18.54±0.04
	373	0–5.4	4th BM	6.37±0.05	9.3±0.3
Expt.[49]	273	0–5.4	Vinet	12.52±0.01	12.9±0.02
	373	0–5.4	Vinet	5.33±0.005	18.78±0.02
	453	0–5.4	3rd BM	0.74±0.01	233±29
	453	0–5.4	Vinet	2.97±0.003	25.36±0.02
DFT-D2.[51]	0	0–6	3rd BM	17.4±1.4	7.9±1.3
	0	0–45	3rd BM	19.2±0.2	7.2±0.1

Theoretically, Wu and her colleagues obtained the isothermal EOS for LLM-105 in the pressure range of 0–50 GPa by first-principles calculations.[50] They observed four structural transformations at 8 GPa, 17 GPa, 25 GPa, and 42 GPa, respectively. The results show that the compressibility in the b axis is significantly greater than those in the a and c axes, in qualitative agreement with the previous results of 0–5.4 GPa.[49] Recently, Manaa *et al.* simulated the isotherm of LLM-105 up to 6 GPa by DFT-D2 method.[51] The calculated EOS agrees well with the experimental data.[49] Fitting the 3rd BM EOS yields $B_0 = 17.4 \pm 1.4$ GPa and $B' = 7.9 \pm 1.3$ for the P–V data up to 6 GPa, but B_0=19.2±0.2 GPa and $B' = 7.2 \pm 0.1$ for the entire P–V data up to 45 GPa. These are somehow higher than the experimental values of B_0=14.6±1.6 GPa by refitting the P–V data in the experimental pressure range of 0–5.4 GPa using the 3rd BM EOS.

3.5. CL-20

Hexanitrohexaazaisowurtzitane (HNIW or CL-20) is currently the densest and strongest energetic organic compound that has practical use. So far, four polymorphs (α, β, γ, and ε) have been observed under ambient conditions and the most stable form is the β phase. Gump *et al.* have investigated the EOS of ε-CL-20 using synchrotron angle-dispersive XRD experiments at room temperature in the pressure range up to 6.3 GPa under both hydrostatic and non-hydrostatic loading conditions.[52] No phase transition was observed within the experimental pressure range for both hydrostatic and non-hydrostatic conditions. They found that the peak positions return to the original ambient pressure positions, meaning a reversible compression process. Fitting the 3rd BM EOS yields $B_0 = 34.3 \pm 0.62$ GPa and $B' = 3.57 \pm 0.31$ for the hydrostatic condition; B_0=27.2±0.22 GPa and $B' = 3.12 \pm 0.14$ for the non-hydrostatic case. Later, they also investigated the temperature effect on the isothermal EOS of ε-CL-20 using the same method in the pressure range of 0–5 GPa and at temperatures below 175 °C.[48,53] A ε–γ phase transition was observed at ambient pressure and 125 °C.[53] The P–V data show the b axis is more compressible than the a and c axes. The 3rd BM EOS fitting for the hydrostatic condition yields $B_0 = 13.6 \pm 2.0$ GPa and $B' = 11.7 \pm 3.2$ at ambient temperature. Recent theoretical results[54] showed $B_0 = 15.58$ GPa and $B' = 9.37$, which are in reasonable agreement with experiments. However, these values at 75 °C change to 11.0±1.3 GPa and 14.0±2.7, respectively. This reduction of B_0 implies that heating to 75 °C increases the compressibility of ε-CL-20.

Theoretically, Xu *et al.*[55] simulated the hydrostatic pressure behavior for ε-CL-20 using DFT within PBE functional. The results show that the compressibility is anisotropic both at low and high pressures and the b axis is most compressible among the three axes. Meanwhile, Byrd and Rice calculated the structural properties of ε-CL-20 under hydrostatic pressure of 0–2.5 GPa using DFT within PW91, PBE, and LDA functional.[24] The results are similar to that for β-HMX discussed above. The EOS parameters of CL-20 are summarized in Table 5 for both experiments and *ab initio* calculations.

Table 5. Isothermal EOS parameters for CL-20, HNS, and TNT using different methods. NH stands for non-hydrostatic.

Form	Method	T/K	P/GPa	EOS	B_0/GPa	B'
ε-CL-20	Expt.[52]	273	0–6.3	3rd BM	34.3±0.63	3.57±0.31
		273	0–6.3 (NH)	3rd BM	27.2±0.22	3.13±0.14
ε-CL-20	Expt.[48,53]	273	0–5.75	3rd BM	13.6±2.0	11.7±3.2
		348	0–5.1	3rd BM	11.0±1.3	14.0±2.7
HNS	Expt.[56,57]	273	0–5.4	3rd BM	11.2±0.66	6.2±0.69
TNT	Expt.[59]	273	0–10	Murnaghan	9.6–10.8	6.6–8.2
				Vinet	7.2–8.8	9.5–12.1
			0–10 (N_2 medium)	Murnaghan	12.8±1.4	7.1±0.8
				Vinet	9.0±1.3	11.6±1.2
			0–10 (NH)	Murnaghan	7.3±0.5	9.6±0.4
				Vinet	7.1±0.5	12.0±0.5

3.6. HNS

Hexanitrostilbene (HNS) is a highly insensitive energetic material. Experimentally, Gump *et al.* determined the EOS of HNS at room temperature in the pressure range of 0–5.4 GPa using angle-dispersive XRD.[56,57] The results show that the a and b axes are more compressible than the c axis and it is also a reversible compression process similar to that of LLM-105.[47] The calculated B_0 and B' are 11.2±0.66 GPa and 6.2±0.69, respectively, using the 3rd BM EOS at ambient condition. We summarize the EOS parameters of HNS in Table 5 for both experiments and *ab initio* calculations.

Theoretically, Zhu *et al.* simulated the structural properties of HNS under hydrostatic pressure of 0–80 GPa using DFT within LDA.[58] Their calculations show that the a axis is the most compressible of all three axes, while the b and c axes remain essentially unchanged with pressure. This means that

the compressibility of HNS is anisotropic. The isotherm was also calculated and it was shown that the volume compression is 50% up to 57 GPa.

3.7. TNT

Trinitrotoluene (TNT) is the first commercially used explosive material. Three non-hydrostatic isothermal compression experiments have been performed for TNT up to 10 GPa at room temperature by Bowden and his colleagues.[59] They obtained zero-pressure isothermal B_0 and B_0' by fitting Murnaghan and Vinet EOS. According to the data set and fitting form used, the B_0 ranges between 7.1 GPa and 10.8 GPa for the non-hydrostatic data (Table 5). It is noteworthy that the non-hydrostatic data are softer than the hydrostatic compression curves. Furthermore, the structural change of TNT is anisotropic under compression, that is, the c axis is most sensitive to compression while the a and b axes are identically sensitive. Most importantly, they ruled out the low phase transition near 2 GPa. DFT-D including vdW correction may show reasonable isotherm of TNT compared with the experimental data.[19]

3.8. TATB

Triamino-trinitrobenzene (TATB) is one of the insensitive and more widely used explosive materials. Olinger and Cady first reported the EOS of TATB in 1976.[60] Recently, the isothermal EOS of TATB has been measured by Stevens *et al*. at room temperature in the pressure below 13 GPa.[61] The results show that all reported isotherms are consistent to approximately 2 GPa, but their experimental values are slightly stiffer than those reported by Olinger and Candy.[60] They used three EOS including Murnaghan, Birch–Murnaghan, and Vinet forms to determine B_0 and B' for TATB. Up to 8 GPa, the average results for B_0 and B' are 14.7 GPa and 10.1, respectively.

Theoretically, Byrd and Rice calculated the structural properties of TATB under hydrostatic pressure of 0–7.0 GPa using DFT within PW91, PBE, and LDA functional.[24] The results are similar to those for β-HMX discussed above. Liu and his colleagues[62] studied the P–V curves under hydrostatic pressure up to 10 GPa using DFT with LDA and GGA. They also found that the P–V curves by LDA are in better agreement with the experimental data than those by GGA.

Due to the important role of the vdW interaction for TATB, the hydrostatic and uniaxial compression of TATB have been studied using DFT with empirical vdW correction.[63] The hydrostatic EOS for V/V_0 of 0.7–1.0 is in good agreement with the available experimental data.[61] They fitted the P–V data below 8 GPa to the 3rd BM EOS to determine $B_0 = 18.7$ GPa, which is close to the experimental value of 13.6 GPa.[61]

Recently, Fedorov and Zhuravlev investigated the hydrostatic pressure effects on the structural properties of TATB below 40 GPa using DFT with empirical and nonlocal vdW correction.[64] The isothermal EOS calculated from these methods are in good agreement with experiments.[61] The 3rd BM EOS yields $B_0 = 13.63$ GPa for DFT-D2, 13.84 GPa for DFT-D3, 20.95 GPa for vdW-DF2, and 14.78 GPa for vdW-DF2-C09, in good agreement with the previous experimental values of 13.6–17.1 GPa.[61]

Xiao's group simulated the room-temperature isotherm in the pressure range of 0–100 GPa using *ab initio* molecular dynamics with and without vdW correction.[65] Their results show that the isothermal P–V curve by DFT-D agrees well with the experimental results[61] (see Fig. 2(c)), whereas that by DFT either underestimates or overestimates the experimental results evidently. Moreover, the DFT-D results show that TATB is chemically stable in the entire pressure range investigated, in agreement with the experiments. But DFT misestimates that TATB decomposes at 50 GPa and polymerizes at 100 GPa. In other words, the vdW correction is necessary and important when the structure of TATB is studied. The EOS parameters of TATB are summarized in Table 6 for both experiments and *ab initio* calculations.

Table 6. Isothermal EOS parameters for TATB using different methods.

Method	T/K	P/GPa	EOS	B_0/GPa	B'
Expt.[61]	273	0–8	Murnaghan	15.7±0.9	8.0±0.5
			Vinet	14.7±0.8	10.0±0.6
			3rd BM	13.6±0.6	12.4±0.3
		0–13	Murnaghan	18.9±0.5	5.9±0.5
			Vinet	17.5±0.6	7.6±0.6
			3rd BM	17.1±0.3	8.1±1.4
PBE.[63]	0	$V/V_0 = 0.7$–1.0	3rd BM	18.7	7.9
DFT-D2.[64]	0	0–40	3rd BM	13.63	11.65
			Vinet	15.14	9.16
DFT-D3.[64]	0	0–40	3rd BM	13.84	8.68
			Vinet	14.33	7.94
vdW-DF2.[64]	0	0–40	3rd BM	20.95	7.31
			Vinet	21.02	7.20
vdW-DF2-C09.[64]	0	0-40	3rd BM	14.78	9.49
			Vinet	15.58	8.32

3.9. PETN

Pentaerythritol tetranitrate (PETN) is known as one of most powerful high explosives. Olinger, Halleck, and Cady measured the isothermal compression of PETN up to 10 GPa using XRD technique.[66] They also calculated the shock compression Hugoniot curve from the isothermal compression. The bulk modulus according to the shock velocity was evaluated to be 8.3 GPa. The EOS parameters of PETN are summarized in Table 7 for both experiments and *ab initio* calculations.

Table 7. Isothermal EOS parameters for PETN and FOX-7 using different methods.

Form	Method	T/K	P/GPa	EOS	B_0/GPa	B'
PETN	Expt.[66]	273	0–10.45	–	8.3	–
PETN-I	PW91.[68]	0	0–10.4	3rd BM	9.1	8.3
	PBE.[17]	0	0–6	4th BM	11.36	–
α-FOX-7	Expt.[69]	273	0–8	2nd BM	17.6±0.4	–
				3rd BM	9.6±1.6	20.8±4.3
	Expt.[70]	273	0–4.14	3rd BM	11.81	11.41
α-FOX-7	HF.[28]	0	$(V/V_0)^{1/3} = 0.92$–1.02	–	12.1	–
	HF.[71]	300		–	15.0	–
α-FOX-7	DFT-D	0	0–4	3rd BM	12.46	12.01

Theoretically, the isothermal EOS under hydrostatic compression to 50 GPa was simulated with ReaxFF and DFT calculations by Oleynik *et al.*[67] The computed isotherms agree very well with the available experimental data.[66] Moreover, Byrd and Rice calculated the structural properties of PETN under hydrostatic pressure of 0-9.16 GPa using DFT within PW91, PBE, and LDA functional.[24] The results are similar to those for β-HMX discussed above.

Conroy and his colleagues studied the constitutive relationships of PETN-I under compression up to $V/V_0 = 0.7$ using DFT within PBE functional.[26,68] Their results show that the isothermal EOS agrees reasonably with the experimental values.[66] By using the 3rd BM EOS,[68] the B_0 and B' are 9.1 GPa and 8.3, respectively, consistent with the experimental values of 9.4 GPa and 11.3.[66] Under non-hydrostatic compression, a correlation between shear stresses and sensitivity was built by comparing the uniaxial compression data with experimental information on the anisotropy of sensitivity to shock-induced detonation for PETN-I.[26,68] The more sensitive the direction is, the greater the shear stresses are. Later, Mota and Cagin calculated the crystal structure of PETN using DFT within PBE functional.[17] The E–V data of PETN were calculated and fitted to the 4th BM EOS to obtain the B_0 of 11.36 GPa, a little higher than the experimental value of 9.4 GPa.[66]

3.10. FOX-7

1,1-diamino-2,2-dinitroethene (DADNE or FOX-7) is an insensitive high-power explosive. The EOS of FOX-7 has been determined below 8 GPa using angle-dispersive XRD experiment by Peiris, Wong, and Zerilli.[69] The results show that FOX-7 exhibits anisotropic compression, with the highest compression along the b axis. The 2nd BM EOS yields $B_0 = 17.6 \pm 0.4$ GPa and the 3rd BM EOS gives B_0=9.6±1.6 GPa and B'=20.8±4.3. Recently, Hunter *et al.* reported the hydrostatic compression of α-FOX-7 up to 4.58 GPa at room temperature using neutron powder diffraction.[70] The EOS of α-FOX-7 has been determined over the range 0–4.14 GPa. There is a phase transition over the pressure range of 3.63–4.24 GPa. By using the 3rd BM EOS, it was obtained that $B_0 = 11.81$ GPa and $B' = 11.41$.

Zerilli and Kuklja simulated the compression curve for FOX-7 under the compression of $(V/V_0)^{1/3} = 0.92$–1.02 using HF approximation.[28] The results show that the isotherm also agrees well with the experimental curve.[69] They evaluated the bulk modulus using the usual thermodynamics relation and obtained $B_0 = 12.1$ GPa, a little lower than the experimental value of 17.6 GPa.[69] Furthermore, the effect of temperature on isotherm of FOX-7 has been discussed.[71] They simulated the isotherm between 0 and 400 K, and the 300 K isotherm agrees very well with the experimental results[69] (see Fig. 2(d)). Interestingly, the calculated B_0 is relatively insensitive to temperature and is 15.0 GPa at ambient conditions, which is close to the experimental determination of 17.6 GPa.[69]

Recently, Xiao's group studied the high-pressure behavior of α-FOX-7 and β-FOX-7 under hydrostatic pressure below 40 GPa using DFT calculations.[72,73] For both α-FOX-7 and β-FOX-7, the compressibility is anisotropic and the b axis is more compressible than the a and c axes. The cell volumes calculated by LDA are compressed by 39.9% when the pressure rises up to 40 GPa. Because of poor description of the vdW interaction by DFT calculations, the EOS of α-FOX-7 has also been investigated below GPa using DFT with vdW corrections.[70] The results show that DFT-D reproduces the experimental trend of the isotherm. The 3rd BM EOS yields $B_0 = 12.46$ GPa and $B' = 12.01$, in good agreement with the experimental values.[70] The EOS parameters of FOX-7 are summarized in Table 7 for both experiments and *ab initio* calculations.

Other than the above mentioned works, there is a lot of experimental and theoretical research on the high pressure behaviors for other energetic materials,[32,40,46,74–80] especially for some new synthesized energetic materials.[81–95] The details will not be discussed in this review.

4. Summary and perspectives

Here we have reviewed the experimental and theoretical progress on the equation of states of ten typical energetic materials. The EOS parameters including bulk modulus and its pressure derivative can be calculated using different EOS formulas. The information from EOS is crucial for the effective prediction of their behaviors during storage, transport, and usage.

Though the high-pressure behaviors of some energetic materials have been successfully characterized by experiments and predicted by theoretical simulations, there are also some open issues. Firstly, few thermodynamic data are measured under high pressure in experiments because the energetic materials become more dangerous as the pressure increases. Hence, the predictions of the high-pressure behaviors of energetic materials by theoretical calculations are hard to verify. Secondly, the results obtained by different theoretical approaches could be inconsistent, even contrary. A criterion for the validity of a theoretical model in the case of lack of high-pressure thermodynamic data is desirable. Finally, defects are intrinsic for realistic crystals including crystalline energetic materials. It would be important to further elucidate the relationship between the high-pressure behaviors of energetic materials and their defects like defect type and defect concentration. This should help us to understand why there is a slight difference between the high-pressure data from different experiments.

References

[1] Peiris S M and Piermarini G J 2008 *Static Compression of Energetic Materials* (Berlin: Springer) pp. 99–101

[2] Agrawal J P 2010 *High Energy Materials: Propellants, Explosives and Pyrotechnics* (New York: John Wiley & Sons) pp. 69–162

[3] Manaa M R 2005 *Chemistry at Extreme Conditions* (New York: Elsevier) pp. 269–326

[4] Sabin J R 2014 *Energetic Materials* (New York: Elsevier Science) pp. 1–332

[5] Murnaghan F 1944 *Proceedings of the National Academy of Sciences of the United States of America* **30** 244

[6] Birch F 1947 *Phys. Rev.* **71** 809

[7] Vinet P, Smith J R, Ferrante J and Rose J H 1987 *Phys. Rev. B* **35** 1945

[8] Poirier J P and Tarantola A 1998 *Physics of the Earth and Planetary Interiors* **109** 1

[9] Cohen R E, Gülseren O and Hemley R J 2000 *American Mineralogist* **85** 338

[10] Holzapfel W B 2002 *High Pressure Research* **22** 209

[11] Lysne P C and Hardesty D R 1973 *J. Chem. Phys.* **59** 6512

[12] Cromer D T, Ryan R R and Schiferl D 1985 *J. Phys. Chem.* **89** 2315

[13] Yarger F L and Olinger B 1986 *J. Chem. Phys.* **85** 1534

[14] Citroni M, Datchi F, Bini R, Di Vaira M, Pruzan P, Canny B and Schettino V 2008 *J. Phys. Chem. B* **112** 1095

[15] Liu H, Zhao J, Wei D and Gong Z 2006 *J. Chem. Phys.* **124** 124501

[16] Zerilli F J, Hooper J P and Kuklja M M 2007 *J. Chem. Phys.* **126** 114701

[17] Mota O U O and Ç ağın T 2011 *Journal of Loss Prevention in the Process Industries* **24** 805

[18] Conroy M W, Oleynik I I, Zybin S V and White C T 2009 *J. Phys. Chem. A* **113** 3610

[19] Sorescu D C and Rice B M 2010 *J. Phys. Chem. C* **114** 6734

[20] Dick J J 1993 *J. Phys. Chem.* **97** 6193

[21] Slough W and Perger W F 2010 *Chem. Phys. Lett.* **498** 97

[22] Yoo C S and Cynn H 1999 *J. Chem. Phys.* **111** 10229

[23] Gump J C and Peiris S M 2005 *J. Appl. Phys.* **97** 053513

[24] Byrd E F C and Rice B M 2007 *J. Phys. Chem. C* **111** 2787

[25] Olinger B W R B, Cady H H 1978 *Symposium international Sur Le Comportement Des Milieus Denses Sous Hautes Pressions Dynamiques; Commissariat a l'Energie Atomique Cnetre d'Etudes de Vajours:* Paris, France 1978 3

[26] Conroy M, Oleynik I I, Zybin S V and White C T 2007 *AIP Conference Proceedings* **955** 361

[27] Conroy M W, Oleynik I I, Zybin S V and White C T 2008 *J. Appl. Phys.* **104** 053506

[28] Zerilli F J and Kuklja M M 2006 *J. Phys. Chem. A* **110** 5173

[29] Zerilli F J and Kuklja M M 2010 *J. Phys. Chem. A* **114** 5372

[30] Qiu L, Zhu W H, Xiao J J and Xiao H M 2008 *J. Phys. Chem. B* **112** 3882

[31] Zhu W, Zhang X, Wei T and Xiao H 2009 *Theor. Chem. Acc.* **124** 179

[32] Zhu W, Zhang X, Zhu W and Xiao H 2008 *Physical Chemistry Chemical Physics* **10** 7318

[33] Lu L Y, Wei D Q, Chen X R, Lian D, Ji G F, Zhang Q M and Gong Z Z 2008 *Molecular Physics* **106** 2569

[34] Lian D, Lu L Y, Wei D Q, Zhang Q M, Gong Z Z and Guo Y X 2008 *Chin. Phys. Lett.* **25** 899

[35] Sewell T D 1998 *J. Appl. Phys.* **83** 4142

[36] Cui H L, Ji G F, Chen X R, Zhu W H, Zhao F, Wen Y and Wei D Q 2010 *J. Phys. Chem. A* **114** 1082

[37] Cui H L, Ji G F, Zhao J J, Zhao F, Chen X R, Zhang Q M and Wei D Q 2010 *Molecular Simulation* **36** 670

[38] Chen J, Long Y, Liu Y, Nie F and Sun J 2011 *Sci. China Phys. Mech. Astron.* **54** 831

[39] Long Y and Chen J 2014 *Philosophical Magazine* **94** 2656

[40] Hooks D E, Hayes D B, Hare D E, Reisman D B, Vandersall K S, Forbes J W and Hall C A 2006 *J. Appl. Phys.* **99** 124901

[41] Peng Q, Rahul, Wang G, Liu G R and De S 2014 *Physical Chemistry Chemical Physics* **16** 19972

[42] Oswald I D H, Millar D I A, Davidson A J, Francis D J, Marshall W G, Pulham C R, Cumming A, Lennie A R and Warren J E 2010 *High Pressure Research* **30** 280

[43] Zhao J, Winey J M, Gupta Y M and Perger W 2006 *AIP Conference Proceedings* **845** 555

[44] Conroy M W, Oleynik I I, Zybin S V and White C T 2008 *J. Appl. Phys.* **104** 113501

[45] Hunter S, Sutinen T, Parker S F, Morrison C A, Williamson D M, Thompson S, Gould P J and Pulham C R 2013 *J. Phys. Chem. C* **117** 8062

[46] Millar D I A, Oswald I D H, Francis D J, Marshall W G, Pulham C R and Cumming A S 2009 *Chemical Communications* **562**

[47] Gump J C, Stoltz C A, Freedman B G and Peiris S M 2009 *AIP Conference Proceedings* **1195** 541

[48] Gump J C and Peiris S M 2008 *J. Appl. Phys.* **104** 083509

[49] Gump J C, Stoltz C A, Mason B P, Freedman B G, Ball J R and Peiris S M 2011 *J. Appl. Phys.* **110** 073523

[50] Wu Q, Yang C, Pan Y, Xiang F, Liu Z, Zhu W and Xiao H 2013 *J. Mol. Model* **19** 5159

[51] Manaa M R, Kuo I-F W and Fried L E 2014 *J. Chem. Phys.* **141** 064702

[52] Gump J C, Wong C P, Zerilli F J and Peiris S M 2004 *AIP Conference Proceedings* **706** 963

[53] Gump J C, Stoltz C A and Peiris S M 2007 *AIP Conference Proceedings* **955** 127

[54] Sorescu D C, Rice B M and Thompson D L 1999 *J. Phys. Chem. B* **103** 6783

[55] Xu X J, Zhu W H and Xiao H M 2007 *J. Phys. Chem. B* **111** 2090

[56] Gump J C, Stoltz C, Mason B P and Heim E M 2012 *AIP Conference Proceedings* **1426** 575

[57] Gump J C 2014 *Journal of Physics: Conference Series* **500** 052014

[58] Zhu W, Shi C and Xiao H 2009 *Journal of Molecular Structure: THEOCHEM* **910** 148

[59] Bowden P R, Chellappa R S, Dattelbaum D M, Manner V W, Mack N H and Liu Z 2014 *Journal of Physics: Conference Series* **500** 052006

[60] Olinger B and Cady H H 1976 *6th Symposium (International) on Detonation*, Coronado, California, USA, August 24–27, 224

[61] Stevens L L, Velisavljevic N, Hooks D E and Dattelbaum D M 2008 *Propellants, Explosives, Pyrotechnics* **33** 286

[62] Liu H, Zhao J, Du J, Gong Z, Ji G and Wei D 2007 *Phys. Lett. A* **367** 383

[63] Budzevich M M, Landerville A C, Conroy M W, Lin Y, Oleynik I I and White C T 2010 *J. Appl. Phys.* **107** 113524

[64] Fedorov I A and Zhuravlev Y N 2014 *Chemical Physics* **436–437** 1

[65] Wu Q, Zhu W and Xiao H 2014 *RSC Adv.* **4** 53149
[66] Olinger B, Halleck P M and Cady H H 1975 *J. Chem. Phys.* **62** 4480
[67] Oleynik I I, Conroy M, Zybin S V, Zhang L, van Duin A C, Goddard W A and White C T 2006 *AIP Conference Proceedings* **845** 573
[68] Conroy M W, Oleynik I I, Zybin S V and White C T 2008 *Phys. Rev. B* **77** 094107
[69] Peiris S M, Wong C P and Zerilli F J 2004 *J. Chem. Phys.* **120** 8060
[70] Hunter S, Coster P L, Davidson A J, Millar D I A, Parker S F, Marshall W G, Smith R I, Morrison C A and Pulham C R 2015 *J. Phys. Chem. C* **119** 2322
[71] Zerilli F J and Kuklja M M 2007 *J. Phys. Chem. A* **111** 1721
[72] Wu Q, Zhu W and Xiao H 2013 *J. Mol. Model* **19** 4039
[73] Xiang F, Wu Q, Zhu W and Xiao H 2014 *Struct. Chem.* **25** 1625
[74] Peiris S M, Pangilinan G I and Russell T P 2000 *J. Phys. Chem. A* **104** 11188
[75] Wu Q, Zhu W and Xiao H 2015 *Struct. Chem.* **26** 477
[76] Li S, Li Q, Wang K, Zhou M, Huang X, Liu J, Yang K, Liu B, Cui T, Zou G and Zou B 2013 *J. Phys. Chem. C* **117** 152
[77] Liu Y, Gong X, Wang L and Wang G 2011 *J. Phys. Chem. C* **115** 11738
[78] Liu Y, Zhang L, Wang G, Wang L and Gong X 2012 *J. Phys. Chem. C* **116** 16144
[79] Wang F, Du H C, Liu H and Gong X D 2012 *Journal of Computational Chemistry* **33** 1820
[80] Liu Y, Du H, Wang G, Gong X and Wang L 2012 *Struct. Chem.* **23** 1631
[81] Ciezak J A 2010 *Propellants, Explosives, Pyrotechnics* **35** 373
[82] Ciezak J A 2010 *Propellants, Explosives, Pyrotechnics* **35** 550
[83] Ciezak J A 2010 *Propellants, Explosives, Pyrotechnics* **35** 24
[84] Ciezak J A 2011 *Propellants, Explosives, Pyrotechnics* **36** 446
[85] Klapötke T M, Mayer P, Miró Sabaté C, Welch J M and Wiegand N 2008 *Inorganic Chemistry* **47** 6014
[86] Klapötke T M and Miró Sabaté C 2008 *European Journal of Inorganic Chemistry* **2008** 5350
[87] Klapotke T M, Miro Sabate C and Rasp M 2009 *Journal of Materials Chemistry* **19** 2240
[88] Klapötke T M, Penger A, Pflüger C, Stierstorfer J and Sućeska M 2013 *European Journal of Inorganic Chemistry* **2013** 4667
[89] Klapötke T M, Petermayer C, Piercey D G and Stierstorfer J 2012 *J. Am. Chem. Soc.* **134** 20827
[90] Klapötke T M, Piercey D G and Stierstorfer J 2011 *Propellants, Explosives, Pyrotechnics* **36** 160
[91] Klapötke T M, Piercey D G, Stierstorfer J and Weyrauther M 2012 *Propellants, Explosives, Pyrotechnics* **37** 527
[92] Klapötke T M and Sabaté C M 2008 *Chemistry of Materials* **20** 1750
[93] Klapötke T M and Sabaté C M 2008 *Chemistry of Materials* **20** 3629
[94] Klapötke T M and Stierstorfer J 2008 *European Journal of Inorganic Chemistry* **2008** 4055
[95] Klapötke T M, Stierstorfer J and Wallek A U 2008 *Chemistry of Materials* **20** 4519